AGU PUBLICATIONS

JGR

Journal of Geophysical Research: Atmospheres

RESEARCH ARTICLE
10.1002/2013JD021425

Key Points:
- Seasonal and interannual variations in tropospheric CO over Hyderabad
- Comparison of aircraft CO profiles with reanalysis and models
- Impact of El Niño and La Niña on CO profiles over Hyderabad

Correspondence to:
V. Sheel,
varun@prl.res.in

Citation:
Sheel, V., L. K. Sahu, M. Kajino, M. Deushi, O. Stein, and P. Nedelec (2014), Seasonal and interannual variability of carbon monoxide based on MOZAIC observations, MACC reanalysis, and model simulations over an urban site in India, *J. Geophys. Res. Atmos.*, *119*, 9123–9141, doi:10.1002/2013JD021425.

Received 24 DEC 2013
Accepted 25 JUN 2014
Accepted article online 27 JUN 2014
Published online 18 JUL 2014

Seasonal and interannual variability of carbon monoxide based on MOZAIC observations, MACC reanalysis, and model simulations over an urban site in India

Varun Sheel[1], L. K. Sahu[1], M. Kajino[2], M. Deushi[2], O. Stein[3], and P. Nedelec[4]

[1]Physical Research Laboratory, Ahmedabad, India, [2]Meteorological Research Institute, Japan Meteorological Agency, Tsukuba, Japan, [3]Forschungszentrum Jülich, Jülich, Germany, [4]CNRS, Université de Toulouse, Toulouse, France

Abstract The spatial and temporal variations of carbon monoxide (CO) are analyzed over a tropical urban site, Hyderabad (17°27′N, 78°28′E) in central India. We have used vertical profiles from the Measurement of ozone and water vapor by Airbus in-service aircraft (MOZAIC) aircraft observations, Monitoring Atmospheric Composition and Climate (MACC) reanalysis, and two chemical transport model simulations (Model for Ozone And Related Tracers (MOZART) and MRI global Chemistry Climate Model (MRI-CCM2)) for the years 2006–2008. In the lower troposphere, the CO mixing ratio showed strong seasonality, with higher levels (>300 ppbv) during the winter and premonsoon seasons associated with a stable anticyclonic circulation, while lower CO values (up to 100 ppbv) were observed in the monsoon season. In the planetary boundary layer (PBL), the seasonal distribution of CO shows the impact of both local meteorology and emissions. While the PBL CO is predominantly influenced by strong winds, bringing regional background air from marine and biomass burning regions, under calm conditions CO levels are elevated by local emissions. On the other hand, in the free troposphere, seasonal variation reflects the impact of long-range transport associated with the Intertropical Convergence Zone and biomass burning. The interannual variations were mainly due to transition from El Niño to La Niña conditions. The overall modified normalized mean biases (normalization based on the observed and model mean values) with respect to the observed CO profiles were lower for the MACC reanalysis than the MOZART and MRI-CCM2 models. The CO in the PBL region was consistently underestimated by MACC reanalysis during all the seasons, while MOZART and MRI-CCM2 show both positive and negative biases depending on the season.

1. Introduction

CO plays an important role in the chemistry of the Earth's atmosphere. The lifetime of CO of about 1–3 months [*Prather et al*., 2001] is due to its reaction with the hydroxyl radical (OH), this reaction being the major sink of OH in the atmosphere. Thus, oxidation of CO has a significant impact on the oxidation capacity of the troposphere. On the other hand, it is an important precursor of ozone (O_3). In areas of sufficient NO_x, such as urban and biomass burning regions, oxidation of CO can lead to formation of O_3 in the downwind of the source region [*Fishman and Seiler*, 1983]. CO is also important in the context of climate change, as it indirectly affects the radiative forcing by affecting concentrations of green house gases like O_3 and CH_4 [*Thompson and Ciccerone*, 1986; *Wigley et al*., 2002].

CO has an important impact on regional and global air quality as a pollutant, due to its relatively long lifetime. For example, CO emitted from the Asian region has been known to affect the remote regions of the atmosphere [*Lelieveld et al*., 2001; *Cooper et al*., 2004; *Sahu and Lal*, 2006; *Srivastava and Sheel*, 2013]. It has been seen that anthropogenic emissions of CO from China could enhance the mixing ratio of CO by about 25 ppbv in Southeast Asia [*Sahu et al*., 2013]. The long-range transport of anthropogenic emissions is seen to contribute 37% of the CO variability observed over a mountain site in Italy [*Cristofanelli et al*., 2013].

Among various sources, oxidation from hydrocarbons accounts for about 50% of the CO production, while in terms of direct emissions the main sources are fossil fuels and biofuels and biomass burning [*Prather et al*., 2001]. In contrast to fossil fuel-based anthropogenic emissions, the biomass burning sources exhibit significant interannual variation due to variability in forest fires, savanna fires, and

agricultural waste [*van der Werf et al*., 2006, 2010]. Traditionally, the major source of CO emission in India is the use of biofuels for domestic purpose (firewood, cow dung, crop residue, and the main fuels for cooking in rural India), followed by coal (which is used in thermal power plant and industries like, steel, and cement) and petrol and diesel consumption.

Various emission inventories have been developed to account for the contributions of the major sources of CO [*Granier et al*., 2011]. The anthropogenic emission estimates among these inventories range from 500 to 600 Tg/yr in the year 2000, with a negative global trend of about 4% for the last decade (2000–2010) as estimated by the Monitoring Atmospheric Composition and Climate CityZen (MACCity) inventory [*Granier et al*., 2011]. This inventory calculates emissions based on a projection of the future emissions, RCP8.5, corresponding to a radiative forcing of 8.5°W in the year 2100. Most of these emission inventories reflect the increasing trend in the regional budget of CO for China and India due to the rapid urbanization and industrial growth [*Granier et al*., 2011; *Ohara et al*., 2007]. For India, an increase in anthropogenic CO emissions from about 50 Tg/yr to 80 Tg/yr has been estimated for the period 1998–2010 [*Granier et al*., 2011].

There are large uncertainties in the CO emission estimates from incomplete combustion, due to spatiotemporal variability of biofuels and biomass burning. The amount of global CO emitted from biomass burning sources could be about 15% higher than from fossil fuel-based sources [*van der Werf et al*., 2006]. Moreover, emissions from biomass burning sources show considerable seasonal as well as interannual variability. The Global Fire Emissions Database, version 3 (GFEDv3) inventory [*van der Werf et al*., 2010] estimated the global annual totals to be in the range of 250 to 600 Tg/yr. Typically, the higher annual emissions from biomass burning sources coincide with a very intense El Niño–Southern Oscillation (ENSO) episode, also seen at regional scales [*Duncan et al*., 2003; *Sahu et al*., 2014]. The 1997–2009 average global fire emissions of CO had a contribution of 44% from Africa and 22% from equatorial and Southeast Asia [*van der Werf et al*., 2010].

Existing long-term measurements of CO have been analyzed to characterize the spatial and temporal variability of this important species [e.g., *Emmons et al*., 2000]. These measurements along with models have helped to estimate the budget of CO in the troposphere on global and regional scales [e.g., *Bergamaschi et al*., 2000; *Duncan et al*., 2007; *Pfister et al*., 2004]. However, measurements are sparse over South Asia where CO emissions from various source are increasing [*Ohara et al*., 2007; *Lawrence and Lelieveld*, 2010; *Kumar et al*., 2011]. Surface observations over India are available only for a few sites in the west [*Lal et al*., 2000; *Beig et al*., 2007], south [*Naja and Lal*, 2002], and north [*Ojha et al*., 2012]. A few campaign mode observations of surface CO are also available over marine regions surrounding India [*Lelieveld et al*., 2001; *Lal et al*., 2007; *David et al*., 2011]. For India, the surface observations have been used to study the seasonality of local CO sources.

Measurements of surface CO, O_3, black carbon, and other aerosols at Hyderabad have been reported [*Mahalakshmi et al*., 2011; *Swamy et al*., 2012]. In these studies, the role of local emissions and meteorology has been briefly presented. However, long-term vertical profile measurements of CO have not been analyzed over South Asia so far, which are crucial to study the effect of long-range transport on the seasonality and interannual variability of CO in the free troposphere. Such measurements of the vertical CO profiles are available from the spaceborne instruments (Measurement of Air Pollution from Satellites (MAPS), Scanning Imaging Absorption Spectrometer for Atmospheric Chartography (SCIAMACHY), Atmospheric Infrared Sounder (AIRS), and Measurements Of Pollution In The Troposphere (MOPITT)), but both resolution and accuracy in the lower troposphere are limited [*Worden et al*., 2013]. Thus, due to the lack of other in situ observations over South Asia, vertical profile observations by aircraft are highly valuable, which can be compared to model results for the free troposphere. Earlier, we have studied the seasonality in CO over Bangkok using Measurement of ozone and water vapor by Airbus in-service aircraft (MOZAIC) aircraft observations which highlight the roles of long-range transport and biomass burning [*Sahu et al*., 2013].

In the present study, we analyze the vertical profiles of CO measured over Hyderabad during the years 2006–2008. The primary objective is to study the causes of variability in tropospheric CO using meteorological data, biomass burning emissions, and back trajectory calculations. We compare the aircraft observations with Monitoring Atmospheric Composition and Climate (MACC) reanalysis (a global forecast model assimilating satellite data) and with simulations by two different models—an offline chemical transport model (Model for Ozone And Related Tracers, version 4 (MOZART-4)) and an online chemical transport model (MRI global Chemistry Climate Model (MRI-CCM2)). Model simulations are important

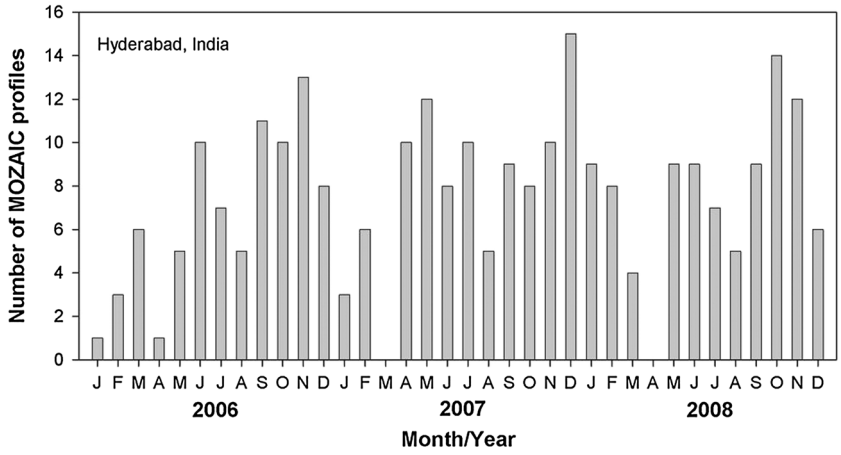

Figure 1. Number of MOZAIC profiles measured over Hyderabad for each month from 2006 to 2008.

especially for regions like India with sparse data coverage (especially vertical profiles). Aircraft-based vertical profiles have the potential to reduce model uncertainties arising from emission inventories and convective parameterization.

2. Observation and Model Simulations

2.1. MOZAIC Data

The MOZAIC (Measurement of ozone and water vapor by Airbus in-service aircraft) program delivered in-flight data of CO and other species from European passenger aircraft since 1994 [*Marenco et al*., 1998]. The species measurements are geolocalized (latitude, longitude, and pressure) and come with meteorological observations (wind direction and speed and temperature). Data acquisition is automatically performed during round-trip international flights (ascent, descent, and cruise phases) from Europe to America, Africa, Middle East, and Asia.

The Thermo Environmental Instrument (Model 48CTL) based on the Gas Filter Correlation technique was used for the measurements of CO. The absorption of infrared radiation at a wavelength of 4.67 μm was used for the detection of CO. A measurement precision of ± 5 ppbv (signal noise), ± 5% (calibration), and minimum detection limit of 10 ppbv were achieved for a 30 s integration time. The analyzers are periodically calibrated in the laboratory using CO ppmv range concentrations in air from compressed cylinders with a National Institute of Standards and Technology specification for CO concentration. A Nafion membrane from Perma Pure, Inc. was installed to dry the air before the measurement. Additional description about the instrument calibration, measurement technique, air drying, and the technical details are described in *Nedelec et al*. [2003]. The MOZAIC program also measures ozone and relative humidity.

The flight observations taken during both takeoff and landing of the aircraft provide the vertical profile data. Measurements of CO are taken every 30 s from takeoff to landing. Raw data (30 s time resolution) are averaged over 150 m height intervals. Profiles are defined as the part of the flight between ground level and the first pressure-stabilized cruising level, usually up to about 300 hPa (200 hPa) with regard to the ascent (descent) profile. Thus, the profile data extend to a maximum of 12 km altitude, as the cruise altitude is predefined by international air traffic regulations. The measuring aircraft does not ascend/descend vertically above a location but that it follows a well-defined flight path before reaching cruise altitude. Below about 4 km, this may not be far from the city, but at higher altitudes, it may extend horizontally to some 200 km from the destination. However, at this height CO does not exhibit much horizontal variability. Therefore, for the purposes of such studies, this variation can be ignored. In this study, we have used about 269 profiles of CO measured over Hyderabad during the years 2006–2008. The histogram of the number of daily MOZAIC profiles in different months is shown in Figure 1. These daily profiles were averaged for a particular month or a season to study the relevant seasonal variability.

2.2. Description of the MOZART Model

MOZART-4 (Model for Ozone And Related Tracers, version 4) is a 3-D global chemical transport model designed to simulate both chemical and transport processes in the troposphere. MOZART-4 simulates comprehensive tropospheric chemistry with 85 gas phase species, 12 bulk aerosol species, 39 photolysis, and 157 gas phase reactions [*Emmons et al*., 2010]. The model has been simulated at a resolution of 2.8° × 2.8° with 28 sigma pressure levels reaching from the surface to about a pressure level of 2 hPa. Meteorological fields from the National Centers for Environmental Prediction reanalysis [*Kalnay et al*., 1996; *Kistler et al*., 2001] have been used in the present work. The emission inventories for major anthropogenic sources, i.e., fossil fuel combustion and biofuel burning used are taken from the Precursors of Ozone and their Effects in the Troposphere (POET) inventory for the year 2000 [*Granier et al*., 2004]. The POET inventory is based on the European projects of the Global Emissions Inventory Activity (GEIA) and the Emissions Database for Global Atmospheric Research [*Olivier et al*., 2003, 2005]. The POET inventory gridded for 1° × 1° includes anthropogenic, fire, and natural emission data. The emission data from fire and natural sources have a monthly variation, while anthropogenic emissions were kept constant. Anthropogenic emissions of CO and NO_x have been updated over Asia with the Regional Emission inventory in Asia (REAS) inventory [*Ohara et al*., 2007] for the year 2006. The monthly averaged biomass burning emissions were taken from the Global Fire Emission Database, version 2 (GFEDv2.0) [*van der Werf et al*., 2006]. At the Physical Research Laboratory, we run the model on the three Teraflops high performance computing Linux cluster with 20 nodes. A typical 1 year run takes about 12 h of wall clock time [*Srivastava and Sheel*, 2013].

2.3. Description of MRI-CCM2 Model

The MRI-CCM2 (MRI global Chemistry Climate Model) is a global chemistry climate model that simulates the distribution and evolution of O_3 and other trace gases in the troposphere and the stratosphere [*Deushi and Shibata*, 2011]. The chemistry module of MRI-CCM2 includes 90 chemical species with 178 gas phase reactions, 59 photolysis reactions, and 16 heterogeneous reactions. The horizontal coordinate of the MRI-CCM2 is a Gaussian grid with a resolution of about 110 km. In the vertical, a hybrid *p-σ* coordinate is used with 64 layers extending from the surface to the mesopause (0.01 hPa ≈ 80 km).

We performed a simulation using the model for the period 2006–2008. Because the simulation used in this study is the same as that in *Sahu et al*. [2014], it is only briefly mentioned here. In the simulation, the horizontal wind field was nudged toward the Japan Meteorological Agency Climate Data Assimilation System (JCDAS) analysis [*Onogi et al*., 2007]. Anthropogenic emission data were taken from the MACCity data set developed as part of two EU projects: MACC and CityZen [*Granier et al*., 2011]. Biomass burning emission data were taken from the Global Fire Emissions Database, version 3 (GFEDv3.0) [*van der Werf et al*., 2010]. Biogenic and oceanic emissions were taken from *Horowitz et al*. [2003, and references therein].

2.4. Description of MACC Reanalysis

The EU-FP7 project Monitoring Atmospheric Composition and Climate (MACC) aims to provide data on atmospheric composition for present conditions and recent years, as well as near real time forecasts of the important atmospheric trace constituents [*Stein et al*., 2012]. MACC composes the atmospheric contribution to Europe's global monitoring initiatives, COPERNICUS (formerly Global Monitoring for Environment and Security).

The global MACC reanalysis is described in *Inness et al*. [2013] and covers the years 2003–2010. European Centre for Medium-Range Weather Forecasts' integrated forecast system (IFS) has been coupled to the version-3 of MOZART [*Flemming et al*., 2009], and both models were run in parallel at the same resolution (60 vertical levels from the surface to 0.1 hPa, 1.125° × 1.125° latitude/longitude). Multiple satellite data for O_3, CO, and NO_2 were assimilated in IFS, which provides basic meteorological data and species initial concentrations to MOZART. In the case of CO, MOPITT total column densities and Infrared Atmospheric Sounding Interferometer (IASI) total columns (from April 2008 onward) have been assimilated regularly [*Inness et al*., 2013]. Chemical reaction equations, emissions, and deposition were calculated in MOZART, and fields were exchanged between MOZART and IFS with a time step of 1 h.

The MACCity inventory of global anthropogenic emissions has been used for the MACC models [*Granier et al*., 2011]. Biogenic emissions are from Model of Emissions of Gases and Aerosols from Nature, version 2

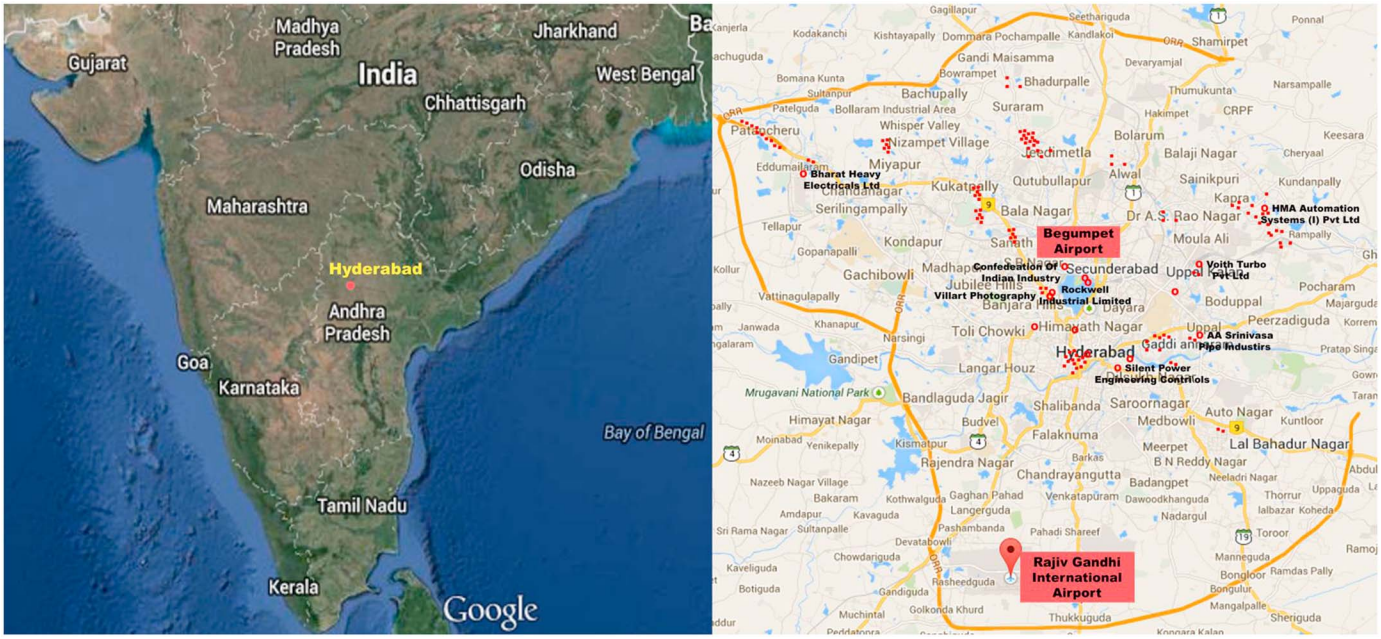

Figure 2. (left) Location of Hyderabad in India and (right) city map of Hyderabad showing location of the two airports and various industries.

(MEGAN-v2) [*Guenther et al.*, 2006], and other natural emissions are from the POET project and GEIA. Biomass burning emissions in the MACC reanalysis for the years up to 2008 are from GVEDv3.0 [*van der Werf et al.*, 2010].

3. Description of Site and Variation in Meteorology

Hyderabad lies at 17°27′N and 78°28′E in the southern peninsular state of Andhra Pradesh in India. The city is situated at a height of around 545 m above the mean sea level and covers an area of 625 km^2. Hyderabad is the fifth largest city of India with a population of about seven million people (2011 census). Rapid urbanization and economic development has encouraged migration into this city, leading to increasing trend in the number of vehicles as well as industries. By March 2011, the number of vehicles in the city reached 2.4 million (http://hyderabad.trafficpolice.co.in/). The transport sector contributes significantly to the air pollution in terms of particulate matter and trace gases. The Andhra Pradesh Pollution Control Board estimated that CO is one of the major pollutants in the city (http://www.appcb.ap.nic.in). CO emissions in the year 2010–2011 for the Greater Hyderabad Municipal Corporation region have been estimated to be 431,000 t yr^{-1} [*Guttikunda and Kopakka*, 2013], equivalent to 60 Kg of CO emissions per capita $year^{-1}$. These emissions are higher than from the Indian metropolitan cities of Mumbai and Kolkata but comparable to Rio de Janeiro [*Gurjar et al.*, 2008]. The city is influenced by urban emissions and also by the transport from biomass burning sources in surrounding rural and suburban regions. The metropolis of Hyderabad was served by the Begumpet Airport until the middle of the year 2008, after which Rajiv Gandhi International Airport became operational. Figure 2 shows the location of Hyderabad in India and the location of the two airports with respect to the city of Hyderabad. A large industrial sector dealing with metal and agroprocessing, paints, tanning, and pharmaceuticals is located in the outskirts of Hyderabad city. Some major industries such as Electronics Corporation of India Limited, Hindustan Cables Limited, and Hindustan Petroleum Corporation Limited are located in the northeast and northwest directions of the airport [*Swamy et al.*, 2012].

Hyderabad has a semiarid climate, with a mixture of wet and dry weather during the hot premonsoon period from March to May, the monsoon season from June to September with a total rainfall of about 800 mm, a post monsoon season (October and November) with well-balanced weather, and a dry winter (December to February). The time series of surface meteorological parameters from January 2006 to December 2008 are shown in Figure 3. These were measured at the national balloon facility of the Tata Institute of Fundamental Research campus located about 15 km from the city center of Hyderabad in the northeast direction. As shown in Figure 3,

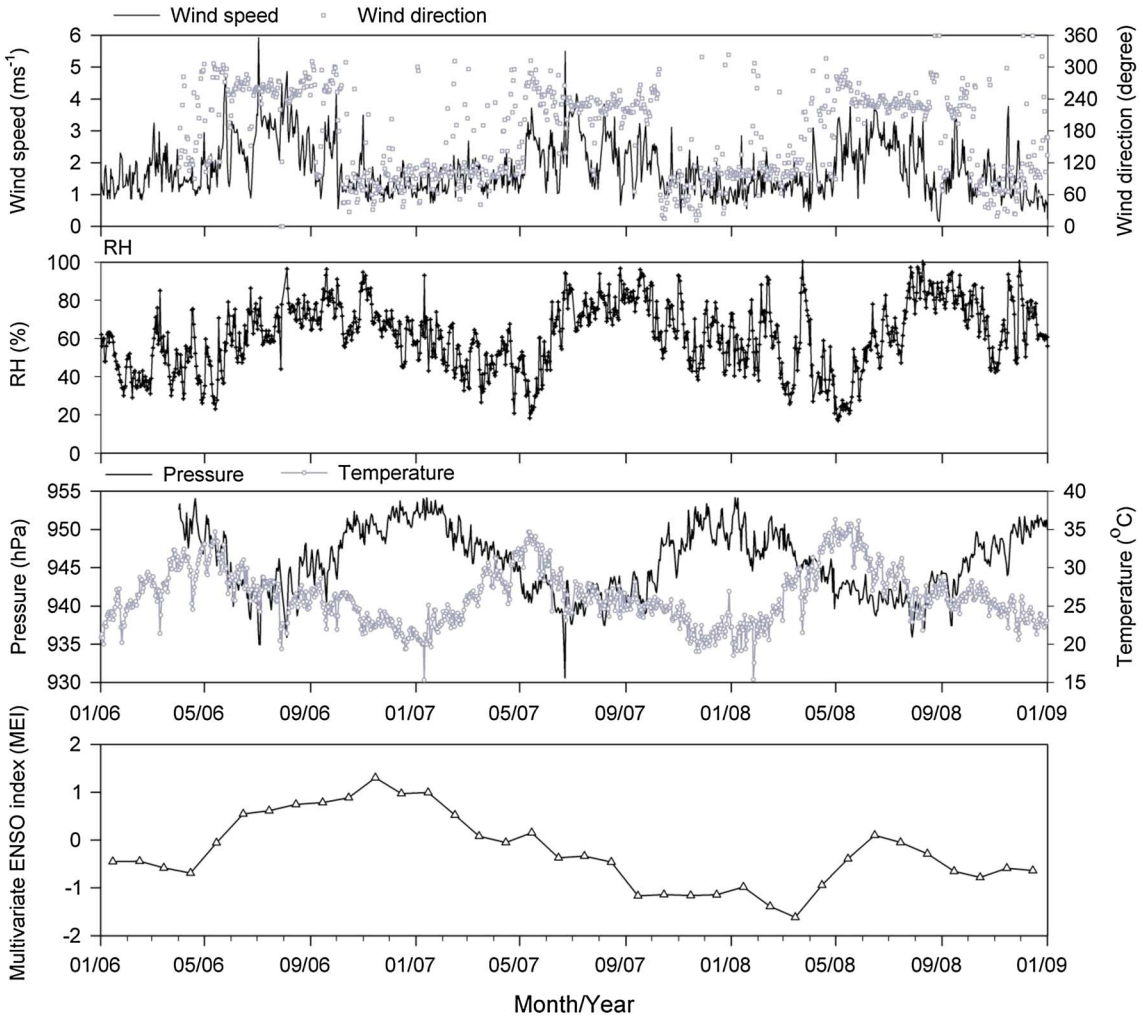

Figure 3. Time series of daily mean meteorological parameters at Hyderabad and monthly ENSO index data during the years 2006–2008.

the daily mean surface temperature over Hyderabad varies from a minimum of typically 15°C in December to a maximum of about 35°C in May and is rarely beyond these two extremes. The temperature does not exhibit any significant interannual variation. The air mass during monsoon comes from southwest direction bringing cleaner air from the Arabian Sea and Indian Ocean with surface wind speeds of about 5 m s^{-1} (Figure 3). In the winter season, winds from the northeast and northwest directions transport continental pollution with surface wind speeds of typically 1–2 m s^{-1}. The premonsoon and post monsoon seasons are the transition period between the monsoon and winter seasons and are thus influenced by mixed air from both marine and continental regions. The winter and premonsoon seasons in Hyderabad are relatively dry compared to the monsoon season. As can be seen in Figure 3, the relative humidity (RH) is high during the monsoon season, with values around 85% in the month of August. RH values as low as 30% are observed during the month of May. The average values of RH for the winter, premonsoon, monsoon, and post monsoon seasons are 61%, 48%, 78%, and 68%, respectively. The sea level pressure variation shows an anticorrelation with temperature in the post monsoon and winter period, with a maximum of about 950 hPa in the winter months. A minimum pressure of 935 hPa is observed during monsoon months.

The phenomena of El Niño–Southern Oscillation (ENSO) are associated with the cyclical warming and cooling of central and eastern Pacific Ocean. Shown in Figure 3 is the multivariate ENSO index, which is based on six parameters: sea level pressure, zonal and meridional components of the surface wind, sea surface temperature, surface air temperature, and cloudiness of the southern Pacific Ocean [*Wolter and Timlin*, 2011]. The large positive values of the index (data for which have been taken from the NOAA website) in 2006,

compared to 2007 and 2008, indicate the transition from the El Niño in the year 2006 to La Niña in the year 2008 [*Sahu et al*., 2014]. ENSO has been observed to have an effect on the Indian summer monsoon. The La Niña conditions, subsequent to El Niño events, are believed to cause positive rainfall anomalies exceeding 1 standard deviation [*Park et al*., 2010].

4. Results

4.1. Vertical Profiles of CO

The vertical profiles of CO for the four seasons over Hyderabad are shown in Figure 4. Some of the general features noticed can be described as follows. In all seasons, the mixing ratio of CO decreases very rapidly (by 150 to 300 ppbv) with altitude in the lowest 1000 m. This decrease is particularly rapid during the winter season as CO mixing ratios decreased from about 500 ppbv to 200 ppbv. In the premonsoon and the post monsoon seasons, the CO mixing ratios decreased more slowly in the lowest 1000 m, from about 400 ppbv at the surface to about 200 ppbv at 1 km. The slope of the vertical profiles is least during the monsoon season, when the surface CO values are low at about 200 ppbv and the winds are high.

We now discuss some seasonal-dependent features seen in the CO variability. The winter season sees the largest variability in the lower troposphere (between 1 and 4 km altitudes) where CO decreases from 200 ppbv to 100 ppbv. Near the surface, calm winds (1–4 m s^{-1}) allow the effect of local pollution to dominate. Above a height of 4 km, strong winds [*Sahu et al*., 2014] help in maintaining the low values of around 100 ppbv. Not much variability in CO mixing ratios is seen from year to year in the upper troposphere. During 2006, there is a high CO event at about 3 km altitude during winter season. This is an El Niño period (Figure 3), and consequently, there is long-range transport of biomass emitted CO from Southeast Asia, as discussed in section 5.1. In the premonsoon season, CO decreases rather slowly with altitude between 1 km and 3 km, whereas above 4 km CO becomes almost constant with a mixing ratio of 100 ppbv. The monsoon season does not see much variation with altitude in the CO profiles in the free troposphere over Hyderabad. From Table 1 (5th–95th percentiles of CO mixing ratios), the highest variability can be seen in the 0–2 km altitude range in premonsoon (178–319 ppbv) and winter (228–416 ppbv). In each season, mixing ratio of CO showed highest variability in the lower troposphere, while the variability was lowest in the middle troposphere.

We have compared the vertical profiles of CO observed during the MOZAIC program with simulations from the MOZART (version 4), the MRI-CCM2 model, and the MACC reanalysis as shown in Figure 4. The profiles from the models are extracted over the grid box nearest to the MOZAIC airport. For all the models and MACC reanalysis, all emissions are interpolated to the model resolution. These models and reanalysis, which have been discussed in the earlier sections, compare better with observations in the free troposphere (above 6 km) during the premonsoon season of all the years and also for the winter season of the years 2006 and 2007. The MRI-CCM2 and MOZART models predominantly overestimate the observed CO in the free troposphere (above 2 km) during all seasons of all the years. On the other hand, MACC reanalysis compares fairly well in the 4–12 km altitude region during the monsoon, post monsoon, and winter seasons of the year 2008. The overall shape of the CO profile is much better reproduced by MACC reanalysis above 1 km altitude, than for the models, which could be an effect of the CO data assimilation in the MACC reanalysis. Apart from these qualitative features, more quantitative features of the comparisons of MOZAIC observations with MACC reanalysis and the models will be presented in the next section.

MACC reanalysis always underestimates the boundary layer CO. The boundary layer CO is overestimated by MOZART as well as MRI-CCM2 in the post monsoon season of all years, while MRI-CCM2 overestimates for the monsoon of all years as well. Disagreement between these two models and the observations in the lower troposphere could partly be due to coarse resolution of the models (2.8° × 2.8° for MOZART and 1° × 1° for MRI-CCM2) and uncertainties in the emission inventories. Another reason of the poor comparison in the boundary layer could be the inability of models to represent subgrid-scale processes of the boundary layer. Other 3-D chemical transport models like GEOS-3 and GEOS-4 are known to underestimate CO in the tropical boundary layer and overestimate in the lower troposphere, compared to aircraft and campaign observations [*Folkins et al*., 2006; *Liu et al*., 2010].

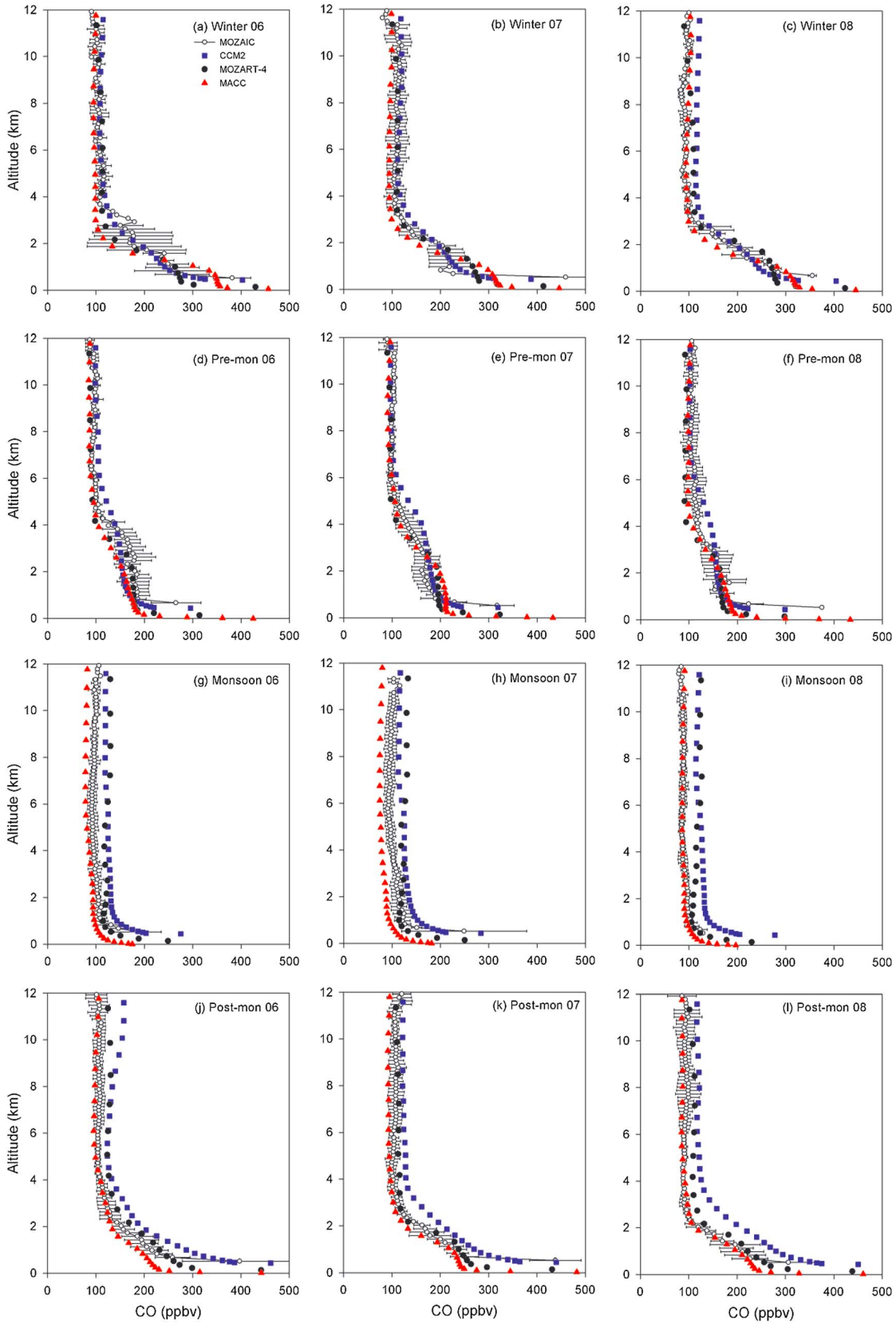

Figure 4. Comparison of season-averaged vertical profiles of CO over Hyderabad during the years 2006–2008, obtained from MOZAIC, MRI-CCM2, MOZART, and MACC reanalysis.

Table 1. Seasonal Averages of 5th–95th Percentiles of the CO Mixing Ratios in Different Regions of the Troposphere for MOZAIC Measurements Over Hyderabad

Altitude Range	Premonsoon	Monsoon	Postmonsoon	Winter
0–2 km	178–319	110–168	190–297	228–416
2–6 km	127–192	94–112	101–142	104–169
6–12 km	97–114	94–109	96–126	102–125

4.2. Seasonal and Interannual Variation in CO

CO concentrations show considerable seasonal and interannual variability over Hyderabad, especially in the 0–2 km altitude range, as can be seen from Figure 5. The box whisker plot shows the monthly mean statistics of the CO mixing ratios in different regions of the troposphere during the years 2006–2008. The CO concentrations are lowest in the monsoon season and highest in the winter season. The seasonal variability decreases with height and so does the variability during a particular month. In the first 2 km of altitude, the CO minimum is observed to be about 100 ppbv during July of 2006–2008, while the maximum value is about 550 ppbv during January 2008. The near-surface wind speeds in July are higher compared to August (Figure 3), leading to a higher diluting effect and hence lower CO in July compared to August. The increasing trend of CO starts somewhat from August, as more frequent episodes of high CO start appearing in August

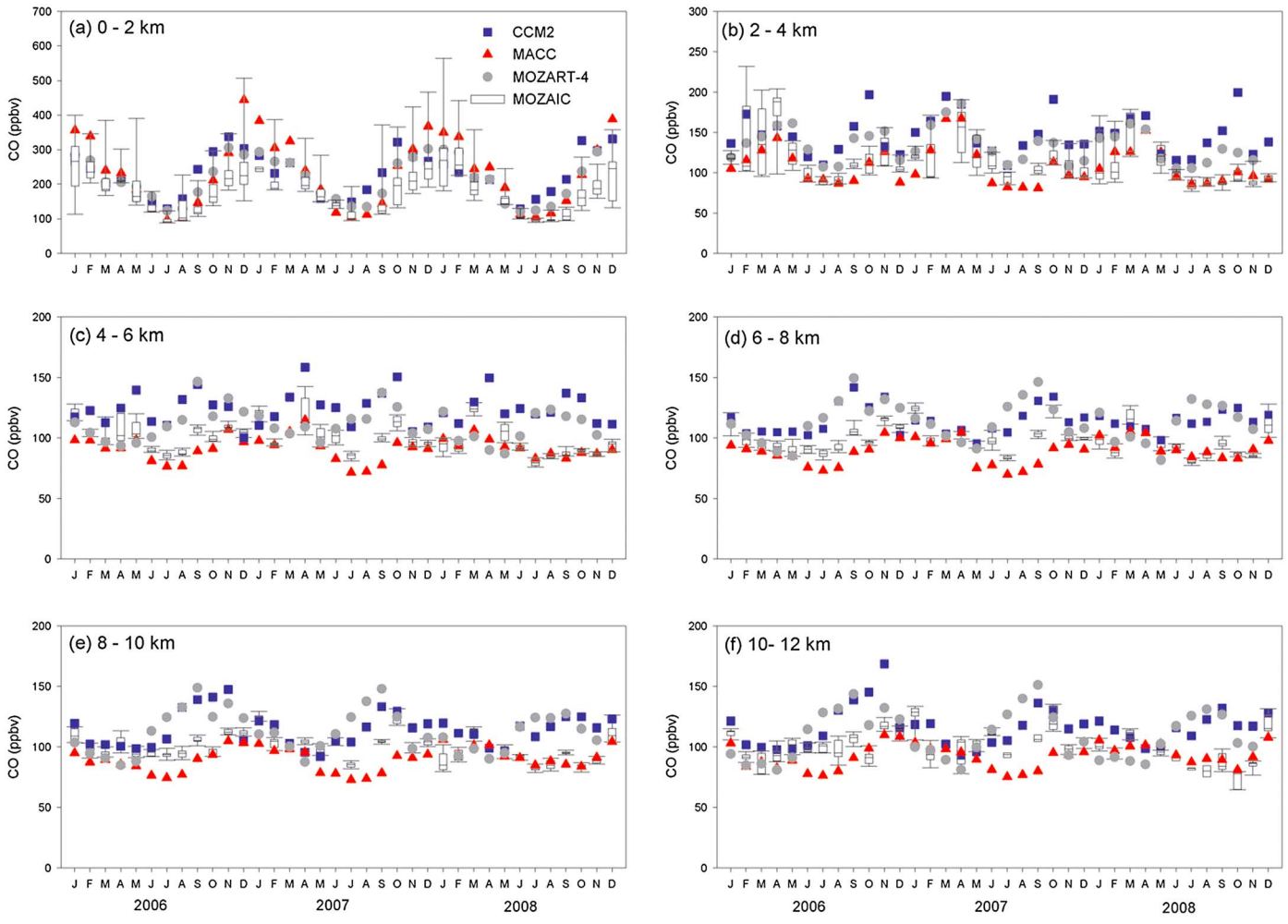

Figure 5. Monthly mean CO in different regions of the troposphere over Hyderabad during the years 2006–2008, using MOZAIC, MRI-CCM2, MOZART, and MACC reanalysis.

Table 2. Modified Normalized Mean Bias of MOZART Model Relative to MOZAIC Observations

Season	0–2 km	2–4 km	4–6 km	6–8 km	8–10 km	10–12 km
Premonsoon 2006	−13.4	−10.9	−10.8	−3.3	−10.4	−7.5
Monsoon 2006	−0.2	18.8	24.3	30.1	28.2	26.9
Postmonsoon 2006	10.0	9.1	17.5	19.0	23.0	16.0
Winter 2006	−4.1	−6.4	3.2	5.5	1.3	−3.6
Premonsoon 2007	−10.4	0.2	−11.5	−4.9	−7.1	−13.0
Monsoon 2007	−6.4	14.4	23.4	29.0	25.9	16.6
Postmonsoon 2007	7.7	0.3	8.5	2.3	0.3	1.5
Winter 2007	2.8	3.7	7.8	4.9	0.6	−2.2
Premonsoon 2008	−13.4	−8.7	−21.1	−14.9	−8.3	−6.4
Monsoon 2008	1.7	19.0	29.2	34.2	32.3	40.6
Postmonsoon 2008	16.2	18.9	21.4	26.7	25.1	25.1
Winter 2008	−2.9	5.9	12.6	12.8	7.5	−7.7

(box whiskers of Figure 5). Extremely high concentrations of black carbon in the boundary layer have also been measured over Hyderabad during winters [*Moorthy et al*., 2013]. In the 2–4 km altitude range, the minimum is again observed in July at about 75 ppbv, while the maximum is 230 ppbv in February 2006. The minimum concentration of CO is found to occur in July at all heights. A maximum of 130 ppbv of CO is observed in April 2007 compared to lowest monsoon levels of 70 ppbv, in the altitude range of 4–6 km. In the other higher altitudes, the CO mixing ratio also varies in the range 70–130 ppbv.

In Figure 5, CO seasonal variability based on MACC reanalysis and as simulated by the MOZART and MRI-CCM2 models are also shown for comparison. In order to take account of large variations in the concentration of species, a useful statistics for model validation is the modified normalized mean bias (MNMB), which is defined as [*Elguindi et al*., 2010]

$$\mathrm{MNMB} = \frac{2}{N}\Sigma_{i=1}^{i=N}\left(\frac{m_i - o_i}{m_i + o_i}\right)\times 100$$

where m_i and o_i represent the model and observed CO concentrations, respectively. N is the total number of data pairs. This method takes care of the asymmetry of the underestimation and overestimation when bias is normalized with respect to mean of the observations. This statistical estimate can lie between −200% and +200% and varies symmetrically with respect to under and over estimation. We use this method to calculate the MNMB for MOZART, MRI-CCM2, and MACC reanalysis, and these are shown in Tables 2–4. The bias is calculated from monthly mean profiles for each season in 2 km altitude intervals from 0 to 12 km. The model profiles are interpolated to the altitudes at which MOZAIC observations are available.

In the boundary layer (0–2 km altitude), the models and reanalysis reproduce the pattern of seasonal cycle very well (Figure 5). It can be seen from Tables 2–4 that the CO in the PBL region was consistently underestimated by MACC reanalysis during all the seasons, with MNMB high in the monsoon season (10–30%) and low in the winter season (2–6%). The match between MACC reanalysis and MOZAIC observations was particularly good for the post monsoon season of the year 2008 (1% bias). On the other

Table 3. Modified Normalized Mean Bias of MACC Reanalysis Relative to MOZAIC Observations

Season	0–2 km	2–4 km	4–6 km	6–8 km	8–10 km	10–12 km
Premonsoon 2006	−19.6	−22.3	−9.3	−6.1	−12.3	−7.9
Monsoon 2006	−20.5	−9.3	−12.5	−18.2	−20.4	−19.2
Postmonsoon 2006	−15.9	−9.3	−4.7	−8.8	−4.3	−3.3
Winter 2006	−2.1	−23.0	−11.0	−11.0	−11.1	−7.4
Premonsoon 2007	−9.9	−7.7	−3.9	−9.0	−15.1	−9.5
Monsoon 2007	−30.5	−25.3	−20.3	−22.4	−24.4	−31.8
Postmonsoon 2007	−7.8	−12.9	−10.0	−17.6	−18.7	−13.0
Winter 2007	−3.3	−13.1	−8.9	−11.2	−11.9	−6.0
Premonsoon 2008	−7.4	−11.8	−12.8	−8.7	−7.7	−2.5
Monsoon 2008	−11.8	−4.3	−1.0	−2.8	−1.4	9.3
Postmonsoon 2008	−1.1	1.9	−0.3	0.4	1.5	5.3
Winter 2008	−6.0	−5.1	1.2	−2.4	3.8	−1.3

Table 4. Modified Normalized Mean Bias of MRI Model Relative to MOZAIC Observations

Season	0–2 km	2–4 km	4–6 km	6–8 km	8–10 km	10–12 km
Premonsoon 2006	−18.9	−8.4	14.0	12.8	3.3	5.7
Monsoon 2006	16.8	24.8	29.3	24.2	19.4	18.8
Postmonsoon 2006	28.6	17.8	18.3	20.3	32.8	36.5
Winter 2006	−2.4	8.7	2.2	1.4	2.3	7.9
Premonsoon 2007	−11.0	2.9	21.7	2.1	−7.5	−7.4
Monsoon 2007	12.3	16.2	25.5	18.4	14.7	3.7
Postmonsoon 2007	22.6	24.8	18.4	10.5	9.6	13.5
Winter 2007	−6.1	17.3	8.3	7.8	8.1	11.9
Premonsoon 2008	−11.3	1.3	6.3	−2.0	−1.3	0.8
Monsoon 2008	27.6	31.8	35.5	26.7	27.2	37.4
Postmonsoon 2008	40.5	42.9	31.6	32.1	33.0	35.6
Winter 2008	−5.2	22.0	20.5	16.3	19.6	14.2

hand, MOZART and MRI-CCM2 models show both positive and negative biases depending on the season. The boundary layer CO is overestimated by MOZART in the post monsoon season of all years, with bias in the range 7–16%. The MRI-CCM2 model overestimates CO for the monsoon season (12–28% bias) and post monsoon season (23–41% bias) of all years. For other seasons, the models predominantly underestimate the observed CO. The comparison of MOZART with MOZAIC observations was particularly good for the monsoon of the year 2006 (0.2% bias).

In the 2–4 km altitude region, the seasonal pattern of CO is reproduced quite well, but the magnitude is not that well simulated by MRI-CCM2 as the simulated minima in the years 2007 and 2008 do not go as low as those observed by MOZAIC. Also, the model shows two maxima and minima in a single year. However, the MACC reanalysis does fairly well. In this altitude range the best match with observations is that of MOZART in the post monsoon season of 2007, with a positive bias of 0.3%. The MOZART and MRI-CCM2 models predominantly overestimate with biases in the range 0.3–19% and 1–43%, respectively. For the MRI-CCM2 model, a high overestimate of about 43% by the model is seen during post monsoon 2008, while the comparison is good during premonsoon 2008 (1.3%).

In the middle troposphere (4–8 km altitude range), the seasonal pattern is again fairly reproduced by the models and especially well by the MACC reanalysis. The MRI-CCM2 model mostly overestimates the observed CO mixing ratios with biases of 1–36% with a particularly good comparison for the winter of the year 2006. In this altitude range, the MACC reanalysis mostly underestimates, though the comparison is particularly good during monsoon, post monsoon and winter seasons of the year 2008, with low biases ranging between −2.8% and +1.2%. The MOZART model overestimates in all the seasons except the premonsoon season, where it underestimates. The MOZART biases are relatively high during the year 2008 (13–30%).

In the upper troposphere (8–12 km altitude range), the amplitudes of seasonal variation by the reanalysis and simulated by the models are much higher than those observed. In this altitude region, the MRI-CCM2 model mostly overestimates with biases in the range 0.8–38%. The MRI-CCM2 model shows a good match to MOZAIC observations (low biases) in the premonsoon season of the year 2008, while the biases in the other seasons of 2008 are particularly high. In the 6–12 km altitude range, the MRI-CCM2 model shows abnormally high peaks of CO during September–November 2006 (Figure 5). This was the El Niño period as indicated by the ENSO index in Figure 3 and the related high biomass burning emissions over Southeast Asia could have been long range transported by the model. These are not captured by the MACC reanalysis nor seen in the MOZAIC observations. In the upper troposphere, the MOZART model underestimates CO in the premonsoon season (with biases 6–13%), while for other seasons and years, it predominantly overestimates. The MOZART biases are relatively high (16–40%) during the monsoon season and low during the winter season (1–7%) and, in particular, the post monsoon season of the year 2007. As usual, the MACC reanalysis predominantly underestimates with relatively low biases in the year 2008 (1–9%) and relatively high biases (9–25%) in the year 2007. In terms of seasonal performance, the MACC maximum percentage biases (19–32%) are in the monsoon seasons of the years 2006 and 2007, while the minimum (1–5%) are in the post monsoon season of the years 2006 and 2008.

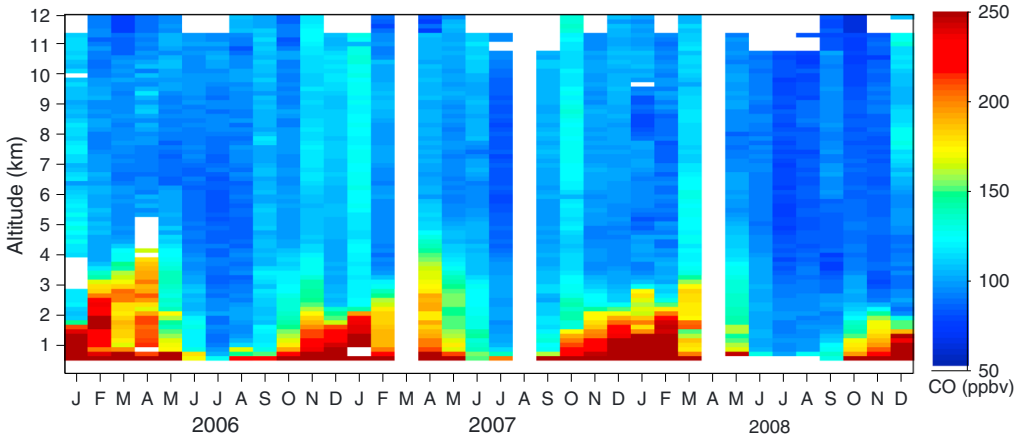

Figure 6. Time versus altitude of monthly mean profiles of CO using MOZAIC observations over Hyderabad, during the years 2006–2008.

The monthly mean MOZAIC and MRI-CCM2 vertical profiles of CO for all the years are shown in Figures 6 and 7, respectively. Both the observation and model show the impact of pollution in the lower tropospheric CO during winter and premonsoon seasons associated with the stable anticyclonic circulation. The ENSO causes subsidence over the western Pacific, creating a low-level anticyclonic circulation over central India

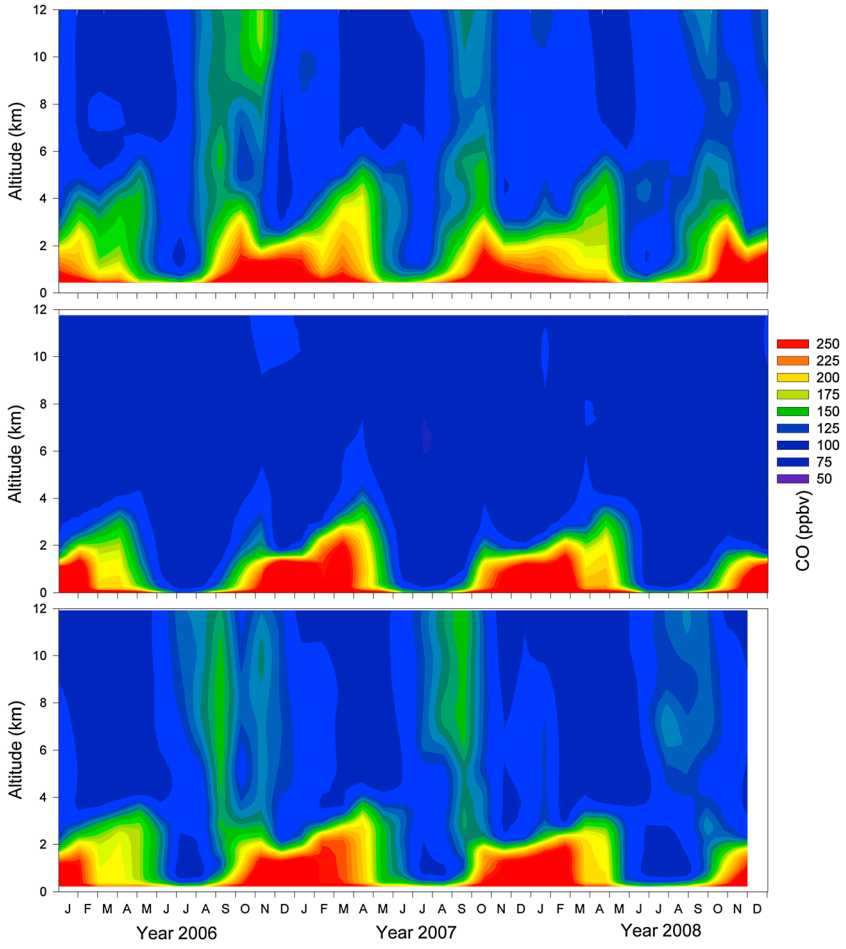

Figure 7. Time versus altitude of monthly mean profiles of CO over Hyderabad during the years 2006–2008, simulated by the (top) MRI-CCM2 and (bottom) MOZART models and from the (middle) MACC reanalysis.

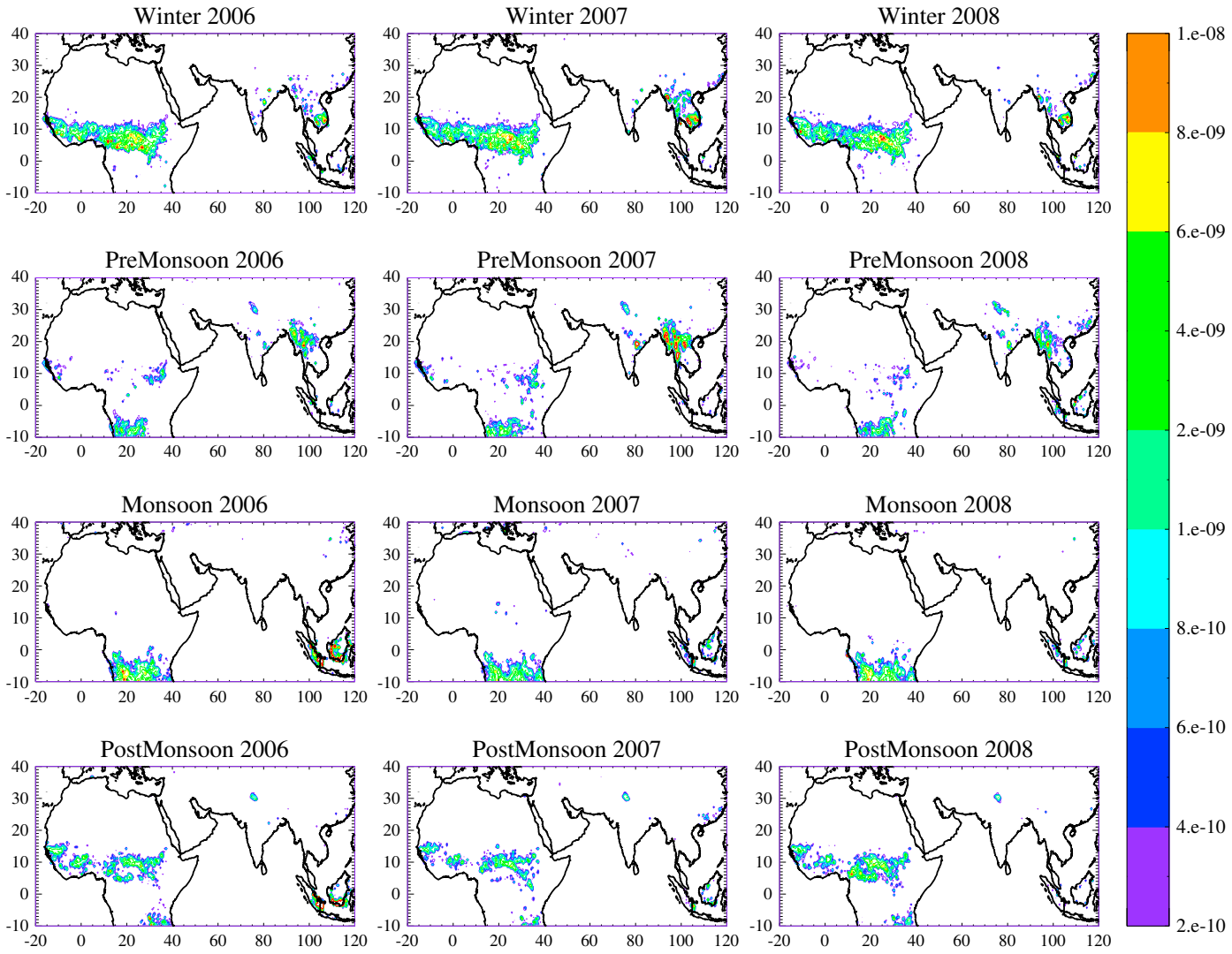

Figure 8. Seasonal mean biomass burning emissions over India and surrounding regions from the GFEDv3.0 emission inventory, for the years 2006–2008.

[*Yadav et al.*, 2010]. This anticyclonic circulation over central India during winter results in strong north easterlies over the peninsula [*Moorthy et al.*, 2013]. As shown in Figure 3, the ENSO index shows the prevalence of an El Niño condition during the year 2006, inhibiting deep convection over peninsular India, possibly due to strong vertical wind shears [*Sahu et al.*, 2014]. It has been seen that the composite outgoing longwave radiation anomalies for El Niño events show suppressed convection over all of India [*Bansoda*, 2011]. On the other hand, La Niña condition prevailed during the years of 2007 and 2008, causing predominant updraft of CO poor marine air from western Pacific region. Consequently, the levels of CO in the upper troposphere during postmonsoon season of year 2006 were higher compared to the same period of the years 2007 and 2008 (Figure 6). This interannual feature was particularly well reproduced by the MRI-CCM2 model simulations (Figure 7).

5. Discussions

5.1. Impact of Biomass Burning and Long-Range Transport

Biomass burning is an important source of CO. It is emitted globally from forest fires and can be transported to long distances. We use the biomass burning emissions estimated by the GFEDv3.0 emission inventory, to study the spatiotemporal variation of the emissions and their possible impact on the CO mixing ratios in

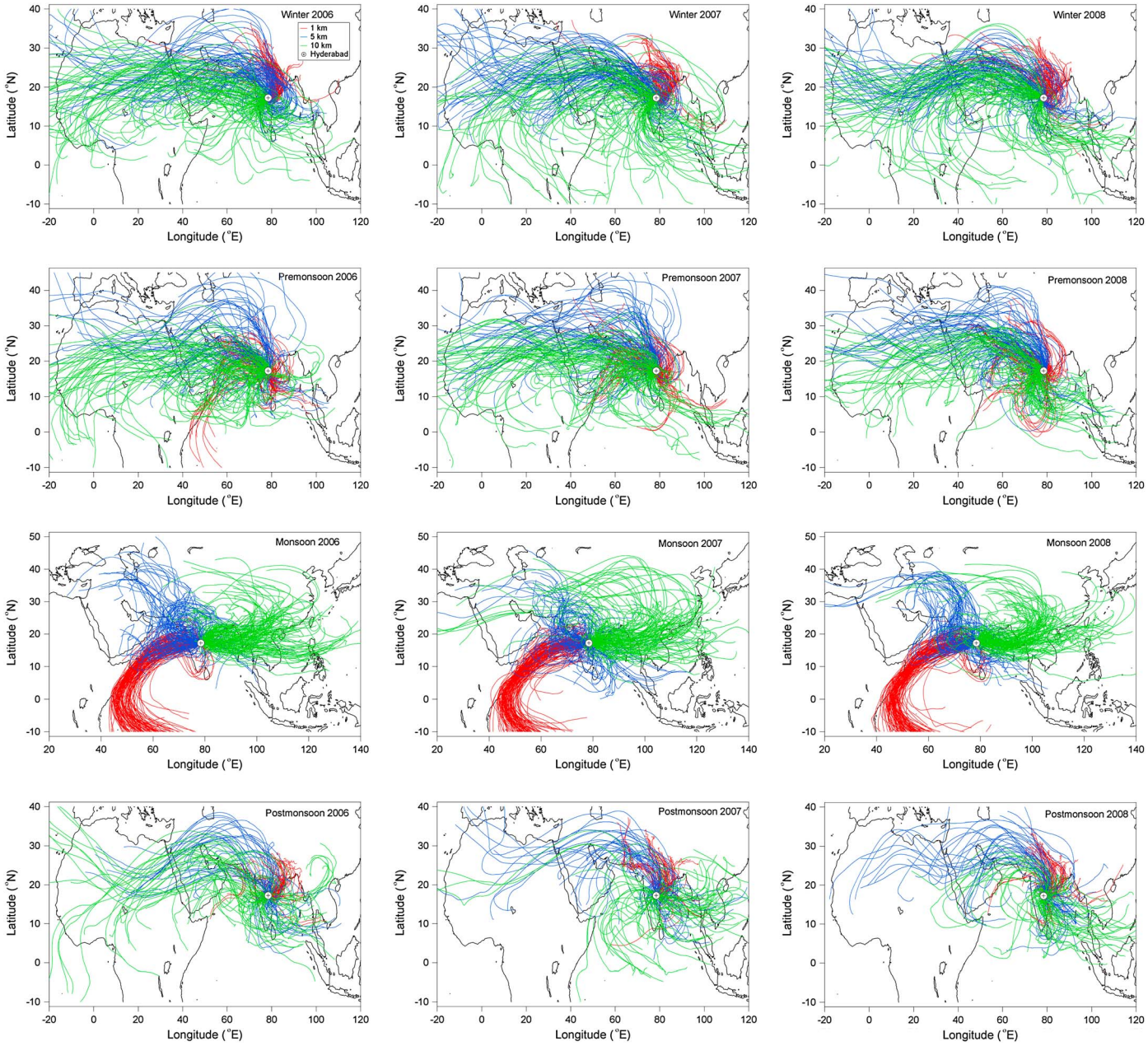

Figure 9. The 7 day back trajectory plots at 1 km (red), 5 km (blue), and 10 km (green) altitude over Hyderabad (encircled symbol) during the different seasons of the years 2006–2008.

Hyderabad. Figure 8 shows the emission maps from GFEDv3.0 for the four seasons used in this study. In the winter season, the biomass burning is highest in the central part of Africa and in the northern countries of Southeast (SE) Asia. This could be a source of contribution to the high values of CO observed during winter over Hyderabad, as Figure 9 shows back trajectories arriving at an altitude of 10 km from the central African region and arriving over Hyderabad in the winter season. Though biomass burning was moderate over peninsular India in winters, it could be a source of the high winter CO values, similar to the increase in the winter values of black carbon that have been observed over Hyderabad [*Moorthy et al*., 2013]. During the premonsoon season, the biomass burning activities shift to the northern part of South-Southeast Asia and intensify over the central Indian subcontinent. In India, biomass burning is highest in the months of March–May. In fact earlier studies have shown that CO in the boundary layer over Hyderabad has been observed to be high during March 2006 due to the active forest fire season over India [*Kharol and Badarinath*,

2007]. In the monsoon season, which is the wet season in Southeast Asia, the biomass burning is mostly confined to the Southern Hemisphere, while it is negligible over central Africa and northern part of South-Southeast Asia (Figure 8). The post monsoon season again sees more biomass burning in the central African region. The biomass burning emissions over Indonesia and Malaysia were much higher during the monsoon and postmonsoon seasons of the year 2006 compared to the corresponding seasons of the years 2007 and 2008. For Indonesia (Malaysia), these emissions were 108.3 (1.2) Tg CO yr^{-1} in the year 2006 compared to 4.6 (0.7) Tg CO yr^{-1} and 0.4 (0.4) Tg CO yr^{-1} in 2007 and 2008, respectively. For the premonsoon season over India, the year 2006 had lower biomass burning than the years 2007 and 2008. These interannual differences in the biomass burning were influenced by the transition from the El Niño in 2006 to the La Niña in 2008. The MOZART-4 model estimates that the SE Asia biomass burning emissions contribute about 20 ppbv of CO at attitudes 9–14 km during July–September 2006 over Hyderabad. The other months and heights had a much lower contribution.

Thus, spatiotemporal variations are seen in the biomass burning emissions over the South-Southeast Asian region. Though this variability in the biomass burning could be an important source of the seasonal variability observed in the vertical profiles of CO over Hyderabad, the pattern in the long-range transport is equally important. We have calculated back trajectories on isentropic surfaces using the Japanese 25 year Reanalysis data from the Japan Meteorological Agency Climate Data Assimilation System (JCDAS), which is 6 hourly and at a resolution of 1.25×1.25 [*Onogi et al*., 2007]. This method uses the advection algorithm of *Draxler and Hess* [1997]. Seven days back trajectories were calculated at 1 km, 5 km, and 10 km altitudes with a time step of 5 min (Figure 9). A clear seasonal pattern can be seen for the trajectories arriving at Hyderabad in different seasons.

In the winter season, the site of Hyderabad is influenced by air from the westerly direction originating from the biomass burning regions of Africa and arriving at altitudes of 5 km and 10 km. These trajectories passed over regions of high biomass burning, as discussed earlier and as seen from emissions in Figure 8. In this season, the air arriving at an altitude of 1 km over Hyderabad originated from the northeast and traveled over the northern Indo-Gangetic plains. The anthropogenic sources in northern India could be a significant source of CO in Hyderabad during winters. In the premonsoon season, the transport pathways of air reaching at 1 km, 5 km, and 10 km altitudes over Hyderabad remain the same as in the winter season. This transport has shown to increase CO in the boundary layer during the premonsoon season [*Mahalakshmi et al*., 2011; *Badarinath et al*., 2010]. During the monsoon season, the boundary layer over Hyderabad shows a clear influence from a southwesterly flow originating from the southern marine regions. This brings moist air from the Indian Ocean and Bay of Bengal with low CO concentrations to Hyderabad. Trajectories at 10 km altitude were traced to originate mostly over central China and the Pacific Ocean, while air arriving at 5 km altitude originated from the northwest, traveling over Afghanistan. In the postmonsoon season, the boundary layer at Hyderabad is again influenced by air mass arriving at 1 km altitude from the northeast, through the Indo-Gangetic plains. The middle troposphere is influenced by air mass arriving at 5 km altitude from western African region. The upper troposphere sees air mass arriving from the land and oceanic regions of Southeast Asia but in 2006 also from northern Africa.

5.2. Impact of Local Meteorology on CO in the PBL

The local meteorology of a region plays an important role in determining the dispersion and accumulation of atmospheric trace species in that region. Meteorological influence on the concentration of CO at urban sites have been observed by wind speed and turbulence and stability of the boundary layer [*McCormick and Xintaras*, 1962; *Elminir*, 2005]. A significant negative correlation has been found between observed wind speeds and CO concentrations in the boundary layer over Hyderabad during different months of the year 2006 [*Badarinath et al*., 2007] and 2008 [*Mahalakshmi et al*., 2011]. We study the dependence of CO mixing ratio on wind speed and direction in the boundary layer ($<$2 km altitude) based on MOZAIC observations. This can be seen in Figure 10, showing polar plots of wind speeds in the four seasons, along with CO mixing ratios in color.

In the PBL region, the observations of CO at Hyderabad were predominantly influenced by the stronger winds from N-SE, SW-NW, west, and N-NE sectors during the winter, premonsoon, monsoon, and postmonsoon seasons, respectively. During all the seasons, however, irrespective of wind direction, the

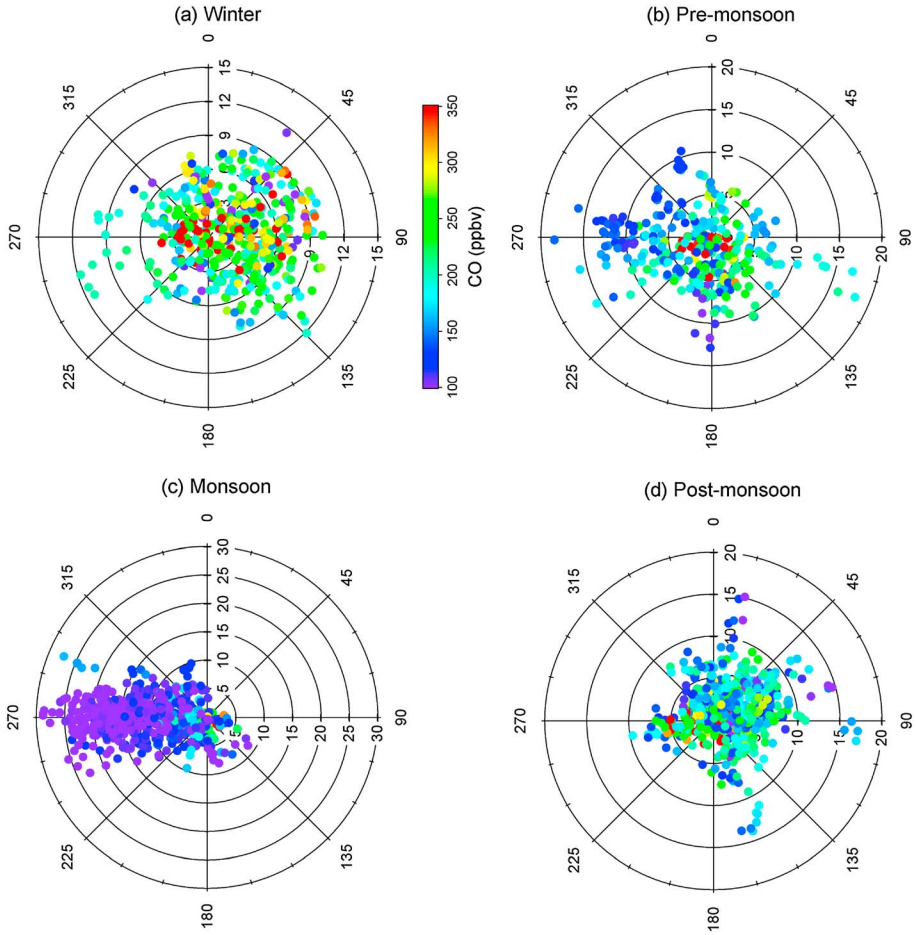

Figure 10. Wind speed (m s^{-1}) and wind direction (deg) polar plot over Hyderabad for the four different seasons 2006–2008, together with CO mixing ratios (ppbv) in color.

mixing ratios of CO were elevated (>300 ppbv) under calm winds (<5 m s^{-1}) due to local pollution. In the stronger wind regimes (>5 m s^{-1}) the impact of dilution due to mixing with regional background (nonlocal) air could be noticed during all the seasons at Hyderabad. In the winter season, observations show highest background CO levels of about 200–250 ppbv. In the monsoon season, lowest background CO levels of about 100–150 ppbv were observed. During the premonsoon and postmonsoon seasons, the dilution took place due to the mixing of air having moderate levels of CO.

The high CO values in winter at Hyderabad are due to both the PBL being shallow in winter and the enhanced biomass burning activities in the surrounding nonlocal regions (Figure 8) from where CO is transported by the strong winds. During the monsoon season, strong surface winds up to 25 m s^{-1} from the west and southwest marine regions bring cleaner air (Figure 10). Moreover, there is no significant biomass burning observed in the surrounding regions during the monsoon season. These factors contribute to the low CO levels observed during the monsoon season. The PBL CO concentrations in the premonsoon season have a contribution from both the surrounding biomass burning and marine regions. In the post monsoon season, regional biomass burning does not contribute to the CO.

6. Summary and Conclusions

We have studied the characteristics of tropospheric CO variability over Hyderabad, an urban location in central India, for the years 2006–2008, based on MOZAIC aircraft measurement, MACC reanalysis, and the models MOZART and MRI-CCM2. The seasonal and year-to-year variations of CO were investigated using

meteorological data, biomass burning emissions, and back trajectory. The four different seasons of winter, premonsoon, monsoon, and postmonsoon are found to be characterized by the distinct variations in the meteorological parameters linked with movement of the Intertropical Convergence Zone. The free tropospheric CO was influenced by long-range transport and biomass burning, while in the PBL, seasonal distribution of CO showed impact of both local regional emissions. Under low winds (<5 m s^{-1}), CO is dominated by local emissions, while strong winds transport regional background air from marine and biomass burning areas. In the lower troposphere, the CO distribution was influenced by the flow of cleaner marine air from SW direction in the monsoon season while the winds from NE and NW directions transport the continental pollutants during the other seasons.

During the local winter, westerly winds from Africa transport CO from areas of extensive biomass burning while over peninsular India, biomass burning is moderate. In the premonsoon season, major biomass burning is seen over India, Thailand, Burma, etc. In the monsoon season, the activities of biomass burning were negligible over the Northern Hemisphere parts of S-SE Asia. In the monsoon and postmonsoon seasons, the significant activities of biomass burning were detected over the island of Indonesia and Malaysia. The year-to-year differences in the biomass burning were caused by the transition from the El Niño to La Niña conditions.

CO exhibits large seasonality in the lower atmosphere with winter season levels of CO above 300 ppbv while values in the monsoon season can go as low as 100 ppbv. Above 4 km the concentrations of CO remain almost constant with altitude, with average values of 103 ± 12 ppbv, 100 ± 12 ppbv, 93 ± 9 ppbv, and 99 ± 14 ppbv in the winter, premonsoon, monsoon, and postmonsoon seasons, respectively. The effect of transition from El Niño in 2006 to La Niña in 2008 on the CO profiles has been seen in the postmonsoon season. In the year 2006, the enhanced levels of CO in the upper troposphere were associated with the El Niño period over Hyderabad. On the other hand, lower values of CO in the year 2008 were associated with the La Niña conditions.

A significant source of uncertainty in the model simulation for near-surface concentrations of species comes from uncertainties in emission inventories and to a lesser extent, the grid resolution. The emission inventories used and grid resolution have been discussed for each model in section 2. For higher altitudes, the convective parameterization is a source of uncertainty. In general, the modified normalized mean biases to the MOZAIC observations are much lower for MACC reanalysis than for MOZART or MRI-CCM2. This can partly be explained by the assimilation of CO total columns from satellites in the MACC reanalysis. MACC reanalysis predominantly underestimates the MOZAIC observations. Such underestimation of CO observations has been earlier attributed to possibly low CO emissions in MACCity inventory [*Stein et al*., 2012]. This results from significant underestimation of traffic CO emissions due to an unrealistic emission reduction in the RCP8.5 scenario for the years 2000–2010. On the other hand, the models MOZART and MRI-CCM2 mostly overestimate the MOZAIC CO profiles over Hyderabad. The model positive biases are particularly high in the free troposphere during the monsoon season. This could be due to less OH formation in the models and hence relatively less loss of CO through oxidation. It has been noticed that MOZART-simulated OH is somewhat lower than the climatology for the tropical regions [*Emmons et al*., 2010]. Model biases are again high in the year 2008, indicating that they are unable to reproduce the La Niña conditions of 2008. On the other hand, biases of MACC reanalysis for 2008 are very low, indicating the importance of data assimilation in representing phenomena like ENSO.

Acknowledgments

The authors would like to thank P.R. Sinha of Tata Institute of Fundamental Research, India, for providing us the surface meteorological data over Hyderabad. Varun Sheel would like to thank Martin Schultz of Forschungszentrum Jülich, Germany, for providing the MACC reanalysis data. M. Deushi would like to acknowledge the JSPS, as this work was partly supported by JSPS KAKENHI grant 24740325. The GFEDv3.0 emission data were downloaded from the ECCAD website.

References

Badarinath, K. V. S., S. K. Kharol, T. R. Kiran Chand, Y. Ganga Parvathi, T. Anasuya, and A. Nirmala Jyothsna (2007), Variations in black carbon aerosol, carbon monoxide and ozone over an urban area of Hyderabad, India, during the forest fire season, *Atmos. Res.*, *85*, 18–26.

Badarinath, K. V. S., S. K. Kharol, D. G. Kaskaoutis, A. R. Sharma, V. Ramaswamy, and H. D. Kambezidis (2010), Long-range transport of dust aerosols over the Arabian Sea and Indian region—A case study using satellite data and ground-based measurements, *Global Planet. Change*, *72*, 164–181.

Bansoda, S. D. (2011), Interannual variability of convective activity over the tropical Indian Ocean during the El Niño/La Niña events, *Int. J. Rem. Sens.*, *32*(19), 5565–5582.

Beig, G., S. Gunthe, and D. B. Jadhav (2007), Simultaneous measurements of ozone and its precursors on a diurnal scale at a semi urban site in India, *J. Atmos. Chem.*, *57*, 239–253, doi:10.1007/s10874-007-9068-8.

Bergamaschi, P., R. Hein, M. Heimann, and P. J. Crutzen (2000), Inverse modeling of the global CO cycle: 1. Inversion of CO mixing ratios, *J. Geophys. Res.*, *105*, 1909–1927, doi:10.1029/1999JD900818.

Cooper, O. R., et al. (2004), A case study of transpacific warm conveyor belt transport: Influence of merging airstreams on trace gas import to North America, *J. Geophys. Res.*, *109*, D23S08, doi:10.1029/2003JD003624.
Cristofanelli, P., F. Fierli, A. Marinoni, F. Calzolari, R. Duchi, J. Burkhart, A. Stohl, M. Maione, J. Arduini, and P. Bonasoni (2013), Influence of biomass burning and anthropogenic emissions on ozone, carbon monoxide and black carbon at the Mt. Cimone GAW-WMO global station (Italy, 2165 m a.s.l.), *Atmos. Chem. Phys.*, *13*, 15–30, doi:10.5194/acp-13-15-2013.
David, L. M., I. A. Girach, and P. R. Nair (2011), Distribution of ozone and its precursors over Bay of Bengal during winter 2009: Role of meteorology, *Ann. Geophys.*, *29*, 1613–1627, doi:10.5194/angeo-29-1613-2011.
Deushi, M., and K. Shibata (2011), Development of a Meteorological Research Institute chemistry–climate model version 2 for the study of tropospheric and stratospheric chemistry, *Pap. Meteorol. Geophys.*, *62*, 1–46, doi:10.2467/mripapers.62.1.
Draxler, R. R., and G. D. Hess (1997), Description of the HYSPLIT_4 modeling system, *NOAA Tech. Memo*, *ERL ARL-224*, December, 24 pp.
Duncan, B., R. Martin, A. Staudt, R. Yevich, and J. Logan (2003), Interannual and seasonal variability of biomass burning emissions constrained by satellite observations, *J. Geophys. Res.*, *108*(D2), 4040, doi:10.1029/2002JD002378.
Duncan, B. N., J. A. Logan, I. Bey, I. A. Megretskaia, R. M. Yantosca, P. C. Novelli, N. B. Jones, and C. P. Rinsland (2007), Global budget of CO, 1988–1997: Source estimates and validation with a global model, *J. Geophys. Res.*, *112*, D22301, doi:10.1029/2007JD008459.
Elguindi, N., et al. (2010), Current status of the ability of the GEMS/MACC models to reproduce the tropospheric CO vertical distribution as measured by MOZAIC, *Geosci. Model Dev.*, *3*, 501–518.
Elminir, H. K. (2005), Dependence of urban air pollutants on meteorology, *Sci. Total Environ.*, *350*, 225–237.
Emmons, L. K., et al. (2000), Data composites of airborne observations of tropospheric ozone and its precursors, *J. Geophys. Res.*, *105*, 20,497–20,538, doi:10.1029/2000JD900232.
Emmons, L. K., et al. (2010), Description and evaluation of the Model for Ozone and Related chemical Tracers, version 4 (MOZART-4), *Geosci. Model Dev.*, *3*, 43–67, doi:10.5194/gmd-3-43-2010.
Fishman, J., and W. Seiler (1983), Correlative nature of ozone and carbon monoxide in the troposphere: Implications for the tropospheric ozone budget, *J. Geophys. Res.*, *88*, 3662–3670, doi:10.1029/JC088iC06p03662.
Flemming, J., A. Inness, H. Flentje, V. Huijnen, P. Moinat, M. G. Schultz, and O. Stein (2009), Coupling global chemistry transport models to ECMWF's integrated forecast system, *Geosci. Model Dev.*, *2*, 253–265, doi:10.5194/gmd-2-253-2009.
Folkins, I., P. Bernath, C. Boone, L. J. Donner, A. Eldering, G. Lesins, R. V. Martin, B.-M. Sinnhuber, and K. Walker (2006), Testing convective parameterizations with tropical measurements of HNO_3, CO, H_2O, and O_3: Implications for the water vapor budget, *J. Geophys. Res.*, *111*, D23304, doi:10.1029/2006JD007325.
Granier, C., et al. (2004), Present and future surface emissions of atmospheric compounds, *European Commission report*, *EVK 2199900011*.
Granier, C., et al. (2011), Evolution of anthropogenic and biomass burning emissions of air pollutants at global and regional scales during the 1980–2010 period, *J. Clim.*, *109*, 163–190, doi:10.1007/s10584-011-0154-1.
Guenther, A., T. Karl, P. Harley, C. Wiedinmyer, P. I. Palmer, and C. Geron (2006), Estimates of global terrestrial isoprene emissions using MEGAN (Model of Emissions of Gases and Aerosols from Nature), *Atmos. Chem. Phys.*, *6*, 3181–3210.
Gurjar, B. R., T. M. Butler, M. G. Lawrence, and J. Lelieveld (2008), Evaluation of emissions and air quality in megacities, *Atmos. Environ.*, *42*, 1593–1606.
Guttikunda, S. K., and R. V. Kopakka (2013), Source emissions and health impacts of urban air pollution in Hyderabad (India), *Air. Qual. Atmos. Health.*, doi:10.1007/s11869-013-0221-z.
Horowitz, L. W., S. M. Walters, D. L. Mauzerall, L. K. Emmons, P. J. Rasch, C. Granier, X. Tie, J.-F. Lamarque, M. G. Schultz, and G. P. Brasseur (2003), A global simulation of tropospheric ozone and related tracers: Description and evaluation of MOZART, version 2, *J. Geophys. Res.*, *108*(D24), 4784, doi:10.1029/2002JD002853.
Inness, A., et al. (2013), The MACC reanalysis: An 8 year data set of atmospheric composition, *Atmos. Chem. Phys.*, *13*, 4073–4109, doi:10.5194/acp-13-4073-2013.
Kalnay, E., et al. (1996), The NCEP/NCAR 40-Year Reanalysis Project, *Bull. Am. Meteorol. Soc.*, *77*, 437–471.
Kharol, S. K., and K. V. S. Badarinath (2007), Effect of synoptic meteorological conditions on aerosol properties over urban environment: A study over tropical urban region of Hyderabad, India, *Acta Geophysica*, *55*, 383–397.
Kistler, R., et al. (2001), The NCEP-NCAR 50-Year Reanalysis: Monthly means CD-ROM and documentation, *Bull. Am. Meteorol. Soc.*, *82*, 247–268.
Kumar, R., M. Naja, S. K. Satheesh, N. Ojha, H. Joshi, T. Sarangi, P. Pant, U. C. Dumka, P. Hegde, and S. Venkataramani (2011), Influences of the springtime northern Indian biomass burning over the central Himalayas, *J. Geophys. Res.*, *116*, D19302, doi:10.1029/2010JD0155059.
Lal, S., M. Naja, and B. H. Subbaraya (2000), Seasonal variations in surface ozone and its precursors over an urban site in India, *Atmos. Environ.*, *34*, 2713–2724, doi:10.1016/S1352-2310(99)00510-5.
Lal, S., L. K. Sahu, and S. Venkataramani (2007), Impact of transport from the surrounding continental regions on the distributions of ozone and related gases over the Bay of Bengal during February 2003, *J. Geophys. Res.*, *112*, D14302, doi:10.1029/2006JD008023.
Lawrence, M. G., and J. Lelieveld (2010), Atmospheric pollutant outflow from southern Asia: A review, *Atmos. Chem. Phys.*, *10*, 11,017–11,096, doi:10.5194/acp-10-11017-2010.
Lelieveld, J., et al. (2001), The Indian Ocean experiment: Widespread air pollution from South and Southeast Asia, *Science*, *291*, 1031–1036.
Liu, J., J. A. Logan, D. B. A. Jones, N. J. Livesey, I. Megretskaia, C. Carouge, and P. Nedelec (2010), Analysis of CO in the tropical troposphere using Aura satellite data and the GEOS-Chem model: Insights into transport characteristics of the GEOS meteorological products, *Atmos. Chem. Phys.*, *10*, 12,207–12,232.
Mahalakshmi, D. V., K. V. S. Badarinath, and C. V. Naidu (2011), Influence of boundary layer dynamics on pollutant concentrations over urban region—A study using ground based measurements, *Indian J. Radio Space Phys.* , *40*, 147–152.
Marenco, A., et al. (1998), Measurement of ozone and water vapor by Airbus in-service aircraft: The MOZAIC airborne program. An overview, *J. Geophys. Res.*, *103*, 25,631–25,642, doi:10.1029/98JD00977.
McCormick, R. A., and C. Xintaras (1962), Variation of carbon monoxide concentrations as related to sampling interval, traffic and meteorological factors, *J. Appl. Meteorol.*, *1*, 237–243, doi:10.1175/1520-0450(1962)001<0237:VOCMCA>2.0.CO;2.
Moorthy, K. K., S. Naseema Beegum, N. Srivastava, S. K. Satheesh, M. Chin, N. Blond, S. Suresh Babu, and S. Singh (2013), Performance evaluation of chemistry transport models over India, *Atm. Env.*, *71*, 210–225.
Naja, M., and S. Lal (2002), Surface ozone and precursors gases at Gadanki (13.5°N, 79.2°E), tropical rural site in India, *J. Geophys. Res.*, *107*(D14), 4197, doi:10.1029/2001JD002477.
Nedelec, P., et al. (2003), An improved infrared carbon monoxide analyser for routine measurements aboard commercial Airbus aircraft: Technical validation and first scientific results of the MOZAIC III programme, *Atmos. Chem. Phys.*, *3*, 1551–1564, doi:10.5194/acp-3-1551-2003.
Ohara, T., H. Akimoto, J. Kurokawa, N. Horii, K. Yamaji, X. Yan, and T. Hayasaka (2007), An Asian emission inventory of anthropogenic emission sources for the period 1980–2020, *Atmos. Chem. Phys.*, *7*, 4419–4444, doi:10.5194/acp-7-4419-2007.

Ojha, N., M. Naja, K. P. Singh, T. Sarangi, R. Kumar, S. Lal, M. G. Lawrence, T. M. Butler, and H. C. Chandola (2012), Variabilities in ozone at a semi-urban site in the Indo-Gangetic Plain region: Association with the meteorology and regional process, *J. Geophys. Res.*, *117*, D20301, doi:10.1029/2012JD017716.

Olivier, J. G. J., J. Peters, C. Granier, G. Petron, J. Müller, and S. Wallens (2003), Present and future surface emissions of atmospheric compounds, *POET Rep. 2*, *EU project EVK2-1999-00011*. [Available at http://www.aero.jussieu.fr/projet/ACCENT/Documents/del2_final.doc.]

Olivier, J. G. J., J. A. Van Aardenne, F. Dentener, V. Pagliari, L. N. Ganzevel, and J. A. H. W. Peters (2005), Recent trends in global greenhouse gas emissions: Regional trends 1970–2000 and spatial distribution of key sources in 2000, *Environ. Sci.*, *2*(2-3), 81–99, doi:10.1080/15693430500400345.

Onogi, K., et al. (2007), The JRA-25 reanalysis, *J. Meteor. Soc. Jpn.*, *85*, 369–432.

Park, H.-S., J. C. H. Chiang, B. R. Lintner, and G. J. Zhang (2010), The delayed effect of major El Niño events on Indian monsoon rainfall, *J. Clim.*, *23*, 932–946.

Pfister, G., G. Pétron, L. K. Emmons, J. C. Gile, D. P. Edwards, J.-F. Lamarque, J.-L. Attie, C. Granier, and P. C. Novelli (2004), Evaluation of CO simulations and the analysis of the CO budget for Europe, *J. Geophys. Res.*, *109*, D19304, doi:10.1029/2004JD004691.

Prather, M., et al. (2001), Atmospheric chemistry and greenhouse gases, in *Climate Change 2001: The Scientific Basis. Contribution of Working Group I to the Third Assessment Report of the Intergovernmental Panel on Climate Change*, edited by J. T. Houghton et al., pp. 239–287, Cambridge Univ. Press, Cambridge, U. K.

Sahu, L. K., and S. Lal (2006), Changes in surface ozone levels due to convective downdrafts over the Bay of Bengal, *Geophys. Res. Lett.*, *33*, L10807, doi:10.1029/2006GL025994.

Sahu, L. K., et al. (2013), Variability in tropospheric carbon monoxide over an urban site in Southeast Asia, *Atmos. Environ.*, *68*, 243–255.

Sahu, L. K., V. Sheel, M. Kajino, M. Deushi, S. S. Gunthe, P. R. Sinha, B. Sauvage, V. Thouret, and H. G. Smit (2014), Seasonal and interannual variability of tropospheric ozone over an urban site in India: A study based on MOZAIC and CCM vertical profiles over Hyderabad, *J. Geophys. Res. Atmos.*, *119*, 3615–3641, doi:10.1002/2013JD021215.

Srivastava, S., and V. Sheel (2013), Study of tropospheric CO and O_3 enhancement episode over Indonesia during Autumn 2006 using the Model for Ozone and Related chemical Tracers (MOZART-4), *Atmos. Environ.*, *67*, 53–62.

Stein, O., J. Flemming, A. Inness, J. W. Kaiser, and M. G. Schultz (2012), Global reactive gases and reanalysis in the MACC project, *J. Integr. Environ. Sci.*, doi:10.1080/1943815X.2012.696545.

Swamy, Y. V., et al. (2012), Impact of nitrogen oxides, volatile organic compounds and black carbon on atmospheric ozone levels at a semi arid urban site in Hyderabad, *Aerosol Air Qual. Res.*, *12*, 662–671.

Thompson, A., and R. Ciccerone (1986), Possible perturbations of atmospheric CO, CH_4 and OH, *J. Geophys. Res.*, *91*, 10,853–10,864, doi:10.1029/JD091iD10p10853.

van der Werf, G. R., J. T. Randerson, L. Giglio, G. J. Collatz, P. S. Kasibhatla, and A. F. Arellano Jr. (2006), Interannual variability in global biomass burning emissions from 1997 to 2004, *Atmos. Chem. Phys.*, *6*, 3423–3441, doi:10.5194/acp-6-3423-2006.

van der Werf, G. R., J. T. Randerson, L. Giglio, G. J. Collatz, M. Mu, P. S. Kasibhatla, D. C. Morton, R. S. DeFries, Y. Jin, and T. T. van Leeuwen (2010), Global fire emissions and the contribution of deforestation, savanna, forest, agricultural, and peat fires, *Atmos. Chem. Phys.*, *10*, 11,707–11,735, doi:10.5194/acp-10-11707-2010.

Wigley, T. M. L., S. J. Smith, and M. J. Prather (2002), Radiative forcing due to reactive gas emissions, *J. Clim.*, *15*(18), 2690–2696.

Wolter, K., and M. S. Timlin (2011), El Niño/Southern Oscillation behaviour since 1871 as diagnosed in an extended multivariate ENSO index (MEI.ext), *Int. J. Climatol.*, *31*, 1074–1087, doi:10.1002/joc.2336.

Worden, H. M., et al. (2013), Decadal record of satellite carbon monoxide observations, *Atmos. Chem. Phys.*, *13*, 837–850, doi:10.5194/acp-13-837-2013.

Yadav, R. K., J. H. Yoo, F. Kucharski, and M. A. Abid (2010), Why is ENSO influencing northwest India winter precipitation in recent decades, *J. Clim.*, *23*, 1979–1993.